Research Article

Removal of Mn from aqueous solutions, by activated carbon obtained from tire residuals

Mohammad Niksirat[1] · **Roohollah Sadeghi**[1] · **Javad Esmaili**[1]

Abstract
Potassium permanganate ($KMnO_4$) is one of the toxic materials that it is essential to remove it from industrial waste waters. In this study, Mn ion was converted to the chelating agent. Tire residuals are used to produce activated carbon. Subsequently, the adsorption of Mn by activated carbon was investigated. The applied activated carbon was prepared by physical activation of the vapor water. Porosity analysis, SEM analysis, zeta potential measurement, adsorption kinetics, and isotherm models were applied to this study. The results showed that the maximum specific surface area of the obtained physical activated carbon was 550 m^2/g. The maximum amount of adsorption was 120 mg/g. It was also shown that the adsorption process is more compatible with pseudo-second-order kinetics model. Isotherm models indicated that the adsorption of Mn on the physically produced activated carbon is more compatible with the Freundlich model. Thermodynamic parameters proved that the adsorption process is spontaneous and endothermic. The overall results demonstrated that activated carbon, obtained from tire residuals, has a good efficacy for removing Mn ions.

Keywords Activated carbon · Tire · Mn · Adsorption · Aqueous solutions

1 Introduction

Environmental pollution caused by hazardous toxic metals is one of important issues [1, 2]. The toxicity of heavy metals is due to their intense tendency to disrupt the vital enzymes in living organisms [3, 4]. Among inorganic pollutants, the heavy metals ions are a serious threat to ecological systems. Some inorganic materials, including salts and ions dissolve in ground waters while passing Mn through the earth's crust can result in some issues. Mn is one of the metal elements that exist in the earth's crust. It can cause many problems. When Mn dissolves in water, it reaches the surface of ground waters. Then it is exposed to the air and becomes insoluble in water. This changes the color of water to brown or red which leads to environmental problems [5–10]. Also, excessive contents of Mn cause damage to the tissues of the nervous system, and result in the neurological disorders [11, 12]. Removing heavy metals from aqueous solutions is considered as an important issue in the public health of society. So far, several methods such as ion exchange, adsorption, reverse osmosis, chemical precipitation, ultrafiltration, and oxidation have been developed for removing heavy metals (like Mn) from aqueous solutions [13–19]. Among these methods, the adsorption procedure is an effective and acceptable method for elimination of Mn [20, 21]. In recent years, several researchers have investigated the adsorption kinetic through studying the adsorption of Mn by using various isotherm models. Rajic et al. [22] used Zeolite Clinoptilolite as an adsorbent to remove Mn ions from aqueous solutions. According to their report, the maximum adsorption capacity of Mn was 10 mg/g. Their results showed that the Langmuir isotherm model as well as the pseudo-second-order kinetic model are more compatible with experimental data. Jusoh et al. [23] used the activated granular carbon to eliminate Fe and Mn. In this study, the reported adsorption capacities of Fe and Mn were 3.6010 and 2.5451 mg/g, respectively. Its

✉ Mohammad Niksirat, niksirat.mohammad@jdeihe.ac.ir | [1]ACECR Institute of Higher Education (Isfahan Branch), Isfahan 84175-443, Iran.

SN Applied Sciences (2019) 1:782 | https://doi.org/10.1007/s42452-019-0797-5

Received: 20 March 2019 / Accepted: 17 June 2019 / Published online: 25 June 2019

former value was higher than the next one. They investigated the Langmuir and Freundlich isotherm models and showed that the Langmuir model has more compatibility with experimental data. Üçer et al. [24] applied composite of activated carbon and tannic acid to eliminating toxic heavy metal ions of Cu, Fe, Cd, Zn and Mn. In their study, according to the Langmuir model, they reported the maximum adsorption capacities for Cu, Fe, Cd, Zn and Mn. The amount of the maximum adsorption capacities was 2.73, 2.80, 2.46, 1.80, and 1.73 mg/g for Cu, Fe, Cd, Zn, and Mn, respectively. According to the previous studies, the maximum adsorption of Mn was 10 mg/g considered as a low value. One of the custom adsorbents is activated carbon. The application of activated carbon is considerable in the industrial scale if its source is available and inexpensive. One of the production sources of activated carbon is tire residuals recognized as one of the most important environmental issues. Most studies have been carried out on the removing colors from aqueous solution by the activated carbon obtained from tire residuals [25–30]. According to the available literatures, there is no research investigating Mn adsorption efficiency by using the activated carbon obtained from tire residuals. According to the previous studies, such activated carbon can possess a high porosity in mesoporous scale if produced in suitable conditions [31–35]. This type of activated carbon can possess enough adsorption potential toward Mn. Mn is one of the metals that can significantly increase its adsorption capacity by converting to a chelating agent [36–43]. Wasay et al. [44–46] separately carried out this work. They enhanced the adsorption capacity by complexing the heavy metals.

In this study, we investigated the physical adsorption of MnO_4 (as a toxic material) in industrial wastewaters. We used activated carbon obtained from tire residuals. Then four various isotherm models, adsorption kinetics, and thermodynamic model were applied based on the obtained results.

2 Materials and methods

2.1 Activated carbon preparation

In this paper, the production of activated carbon from rusty tires through physical methods were investigated. The raw material used for preparing the activated carbon was rusty tires obtained from a rusty tire collection centers in Esfahan, Iran. First, the rusty tires was dried at 50 °C for 24 h until no further weight loss could be detected. Subsequently, it was crushed with a grinder, and sieved. Preparation overview of activated carbon is showed in the Fig. 1.

The preparation of the activated carbon from rusty tire was comprised of two main steps:

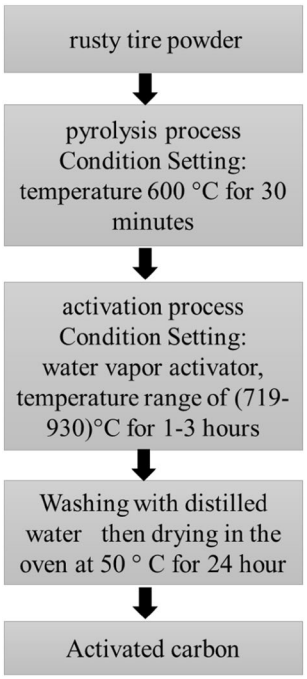

Fig. 1 Scheme of preparation steps of the activated carbon from rusty tire

(a) Pyrolysis processes were performed under a temperature in 600 °C for 30 min, and steady-state flow of nitrogen (inert) gas with a flow rate of 70 ml/min, and at a constant heating rate of 5 °C/min.
(b) Activation processes were performed under a temperature range of (719–930) °C for 1–3 h, and steady-state flow of water vapor activator with a flow rate of 50 ml/min, and at a constant heating rate of 10 °C/min. Subsequently, extensive washing with distilled water, the activated carbon was oven dried at 100 °C for 24 h, and hand milled to a particle size ≤ 200 µm.

2.2 Activated carbon characterization

In order to investigate the surface area of pores, the adsorption and desorption porosimetry measurements were analyzed by using Bel Belsorp mini II model. Morphological characterizations were performed by scanning electron microscopy (SEM) using a field emission TESCAN Vega3 microscope (Czech Republic). Zeta potential of activated carbon sorbents was measured at 298 K using a zeta potential analyzer Malvern Zetasizer (Model: ZEN 5600-Made in UK). 0.01 g activated carbon sample was added into 100 ml of 0.01 M NaCl solution under stirring. The pH value of the mixture was then adjusted to a value between 2 and 11 using 0.1 M HCl or 0.1 M NaOH solutions and the particles were dispersed in a Probe Sonicators for 15 min. After this, around 2 ml sorbent

suspension was drawn for analysis. Seven zeta potential readings were taken and the average zeta potential at a certain pH value was plotted against pH over the range from 2 to 11. The isoelectric point (IEP) was taken as the point where the electrokinetic potential was zero.

2.3 Adsorption studies

$KMnO_4$ was used to study the kinetic adsorption, adsorption isotherms, and thermodynamics. The china made-spectrophotometer (2601-VU-HGIELYAR model) with a maximum wavelength (λ) of 525 nm was used to determine the concentration of MnO_4. The production of chelating agent, MnO_4, was carried out by the following procedure. The potassium permanganate ($KMnO_4$) solution was prepared by dissolving reagent grade $KMnO_4$ in double-distilled water. Then boiling and filtering the solution using a fine glass frit to remove MnO_2. The storage and standardization of MnO_4 solution were the same as the previous description [47]. The kinetic experiments were performed to discover the equilibrium time. For this purpose, the kinetics experiments were carried out for 10–240 min. In this way, 0.025(g) adsorbent was dissolved in 50 ml of a solution containing 50 ppm MnO_4. Then this solution was poured into a shaker according to the specified periods and left in ambient temperature to settle. Then the concentration of the remaining Mn in the solution was calculated by spectrophotometer. The amount of Mn adsorbed on the adsorbent and its removal efficiency can be calculated from Eqs. 1 and 2, respectively.

$$q_e = \frac{(C_o - C_e)V}{M} \tag{1}$$

$$\eta = \frac{(C_o - C_e)}{C_o} \times 100 \tag{2}$$

In the above equations, q_e, is the amount of adsorbed Mn per 1 (g) adsorbent, V is the solution volume, M is the adsorbent mass and C_e is the equilibrium concentration. In this study, different kinetic models, including first-order, second-order, particle-diffusion, and Elovich models were used to describe the data. Also, adsorption isotherm experiments and thermodynamic studies were performed at three temperatures of 25, 40, and 55 °C. The aim of these experiments was to determine the optimum temperature. The Langmuir, Freundlich, Temkin, and Dubinin–Radushkevich (D–R) models were applied for data analysis.

2.4 Kinetic models

In order to investigate the adsorption mechanisms, such as chemical reaction, diffusion control, and mass transfer, several kinetic models were used in different experimental conditions.

In this paper, the kinetic models, including pseudo-first-order, pseudo-second order, intra-particle diffusion, and Elovich were investigated.The pseudo-first-order model is expressed by Eq. 3:

$$\log\left(q_e - q_t\right) = \log q_e - k_1 * t \tag{3}$$

where q_t is the adsorbent capacity at different periods, q_e is the adsorbent capacity at equilibrium time, and k_1 is the reaction rate constant of the pseudo-first-order model [48]. If $\ln(q_e - q_t)$ is drawn against time for laboratory conditions, a straight line will be obtained from which the rate constant, k_1, and the adjusted determination coefficient, R^2_{Adj}, can be determined. The linear form of pseudo-second order, is written as follows:

$$\frac{t}{q_t} = \frac{1}{k_2 q_e^2} + \frac{t}{q_e} \tag{4}$$

$$h = k_2 q_e^2 \tag{5}$$

where k_2 is the rate constant and h is the initial adsorption rate. By plotting t/q_t against t, k_2 and R^2_{Adj} can be calculated [49, 50]. Intraparticle diffusion is a transition process that describes the locomotion of a mass portion from solution to the solid phase [51]. The diffusion and intraparticle model can be represented as follows:

$$q_t = k_i t^{0.5} + C \tag{6}$$

C and k_i in Eq. (6) are used to interpret the chemical kinetics. This model is expressed as follows:

$$q_t = \frac{1}{\beta}\ln(\alpha\beta) + \frac{1}{\beta}\ln t \tag{7}$$

α and β in Eq. 7 are initial adsorption and desorption rate constants of a surface wide coating and activation energy of the chemical adsorbent, respectively [51].

2.5 Equilibrium models

The adsorption isotherm can be described by some models. The parameters related to these models provide important information, for example about internal bonds of adsorbent, adsorption mechanism, and surface characteristics [51, 52].

Freundlich isotherm model can be used to describe heterogeneous adsorption system as follows:

$$\ln q_e = \ln k_f + \frac{1}{n}\ln c_e \tag{8}$$

n and k_f are the Freundlich constants that indicate the maximum capacity of adsorption and inhomogeneity, respectively. The Langmuir model is successfully used for many single-layer adsorption processes. The adsorption is assumed to occur in specific homogeneous sites of adsorbent. This model can be expressed by below equation:

$$\frac{c_e}{q_e} = \frac{1}{k_l q_{max}} + \frac{c_e}{q_{max}} \tag{9}$$

where q_{max} is the maximum capacity of adsorption, k_l is the Langmuir adsorption constant, and R_L is the dimensionless parameter that assesses the type of adsorption process [52].

The Dubinin–Radushkevich model is applied to specify the physical and chemical adsorptions. It can be expressed as follow:

$$\ln q_e = \ln q_m - \beta\varepsilon^2 \tag{10}$$

in which q_m is the maximum capacity of adsorption of metal ions, β is the constant pertained to the average energy of adsorption, and ε is expressed by Eq. 11.

$$\varepsilon = RT \ln\left(1 + \frac{1}{c_e}\right) \tag{11}$$

in which R is the gas constant (8.314 J/mol K), and T is temperature. The free energy of transferring 1 mol of solute from infinity to the adsorbent surface, i.e. the average energy of E, can be achieved by the following equation:

$$E = \frac{1}{\sqrt{2\beta}} \tag{12}$$

Temkin isotherm is another model based on the hypothesis that reduces the adsorption capacity. It is resulted from decreasing the temperature in an adsorbent whose surface coating is linear, rather than logarithmic. This model is represented as follows:

$$q_e = \frac{RT}{b_T} \ln(AT) + \frac{RT}{b_T} \ln c_e \tag{13}$$

where b_T and A, are Temkin constant of adsorption heat, and adsorption potential, respectively [52].

2.6 Thermodynamic study

Another criterion that is particularly important in describing the adsorption process is to determine the thermodynamic parameters of adsorption. The adsorption thermodynamic estimation was performed by the standard values of Gibbs free energy change (ΔG, kJ mol^{-1}), enthalpy change (ΔH, kJ mol^{-1}), and entropy change (ΔS, kJ mol^{-1} k^{-1}). These values were estimated by Eqs. 14 and 15 [53]. The standard Gibbs free energy indicates the adsorption process spontaneity, the standard enthalpy change indicates the adsorption heat, and the standard entropy change represents the organization of adsorbate molecules.

$$\Delta G = -RT \ln K \tag{14}$$

$$\ln K = -\frac{\Delta H}{RT} + \frac{\Delta S}{R} \tag{15}$$

where R is universal constant (kJ mol^{-1} k^{-1}), T is temperature (K), and K is the thermodynamic constant (dimensionless), which was estimated from the parameters of the best fit equilibrium model [54].

3 Results and discussion

In this study, the adsorption process was investigated in the chelating form by using activated carbon obtained from rusty tires. Adsorption and desorption porosimetry, SEM analysis, zeta potential measurement, adsorption kinetics, isotherms, and thermodynamics analysis are performed in this research. The results of the analysis are discussed as follows.

3.1 Characterization of the activated carbon

3.1.1 BET analysis

Figure 2 represents the results of adsorption and desorption porosimetry analysis. Figure 2a and b display the diagram of surface area in the surface specific area analysis, and diagrams of adsorption and desorption isotherm, respectively. In Fig. 2b, the variations of partial pressure are plotted against the total pressure toward the absorbed gas volume in standard conditions. From the results of Fig. 2a and porosimetry analysis, the specific surface area, the total volume of pores, their size were 550 m^2/g, and 1.2232 cm^3/g and 8.8923 nm, respectively. The results of the specific surface area analysis showed that the vapor–activator agent can create pores in the size of meso and micro on activated surface of carbon obtained from rusty tire. Water vapor can also be regarded as a prospering activator for surface production on the activated carbon obtained from rusty tire, using physical method. The total volume and the size of pores indicate that a significant number of pores are micro sized.

As shown in Fig. 2b, the analyzed isotherm has also a hysteresis ring [55]. According to studies and the type of hysteresis ring, it can be stated that the geometric shape of the pores is created by water vapor. The activated carbon, investigated in adsorption and desorption porosimetry

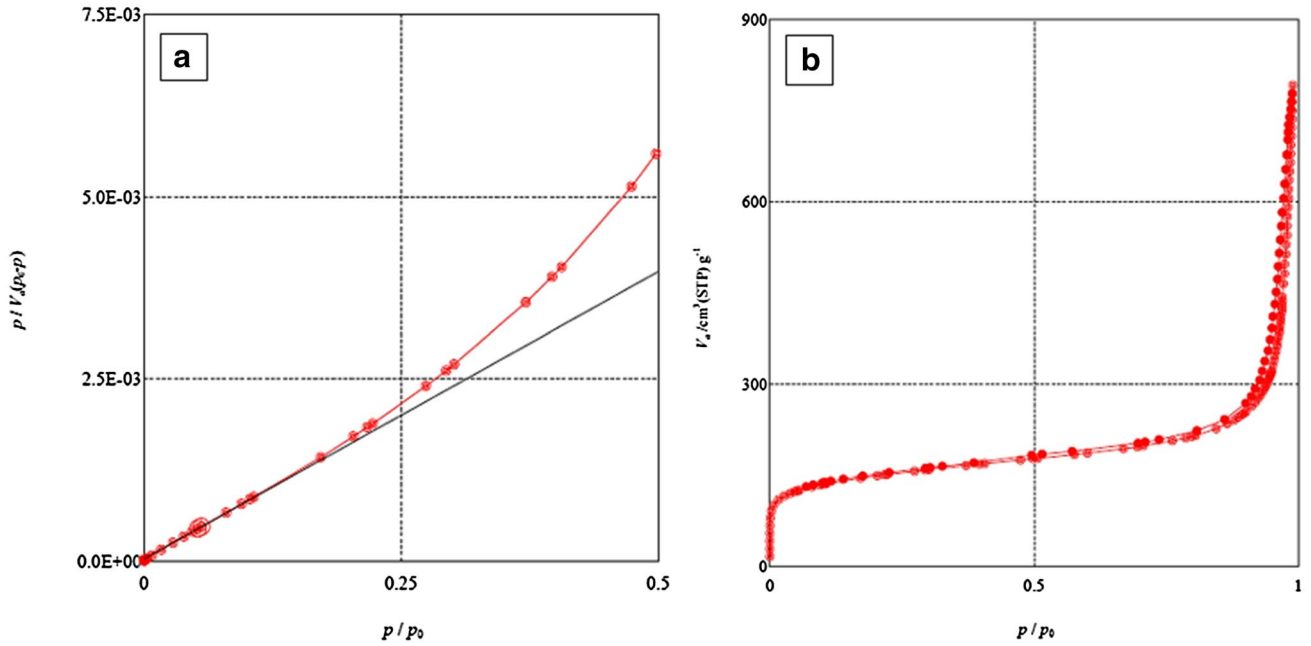

Fig. 2 **a** Plot of the specific surface area; **b** adsorption and desorption isotherm curve

analysis, was produced under optimum conditions of activating temperature, activating period, and water vapor activator.

3.1.2 SEM images

SEM analysis was used to evaluate the surfaces and appearance of the samples. Figure 3a shows the surface morphology of Pyrolysis char before activation. As shown SEM images of the activated carbon after steam activation in magnifications 1Kx, 1Kx, 5.5Kx, 3Kx, and 20 Kx respectively are represented in Fig. 3b–f, it can be observed that correspondingly, a rugged surface and highly irregular is observed and also there are highly scattered irregular cavities on the surface, which may have been due to the destruction of the volatile components and the activation by steam surface under heating.

3.1.3 Zeta potential measurement

Zeta potential is the potential difference between the dispersion medium and the stationary layer of fluid attached to the dispersed particle. It can be used to determine the acidity or basicity of the adsorbent surfaces. The surface charge of activated carbon is determined by the nature of surface groups and solution pH, which could be characterized by the isoelectric point (IEP). pH_{IEP} of activated carbon particles is the pH at which activated carbon surface carries no net electrical charge and could be found by plotting the average zeta potential against the pH value. The point where the curves cross the X-axis, at zero voltage, is taken as the isoelectric point. Figure 4 presented the zeta potential distribution of activated carbon at the pH range from 2 to 11. The pH_{IEP} of activated carbon was around 2.7. It was found that the surface of the activated carbon particles were positively charged at pH values below the pH_{IEP} and negatively charged at pH values above the pH_{IEP}.

As shown in Fig. 4, a wide range of pH has a negative zeta potential. The negative zeta potentials can arise from acidic functional groups, e.g., carboxyl and phenolic hydroxyl groups [56] on the surface of activated carbon. Also, the negative zeta potential shown that small particles in suspension resist aggregation and tend to disperse homogeneously in the solution. Homogeneous dispersion of the adsorbent particle can obviously benefit for improving the adsorption efficiency of the adsorbent.

3.2 Kinetic of adsorption

Understanding the kinetics of adsorption of a certain adsorbate on an adsorbent is essential since the rate of adsorption (that is one criterion of the efficiency of adsorption process). Also, the kinetics of adsorption is essential for the establishment of the mechanism of adsorption. Kinetic studies can give valuable information about the whole adsorption process including operation control and evaluation of the adsorbent Efficiencies [57, 58]. The suitability each model was evaluated by analyzing the adjusted determination coefficient (R^2_{Adj}) [59, 60]. An R^2_{Adj} value close to 1.000 means that the experimental and theoretical q

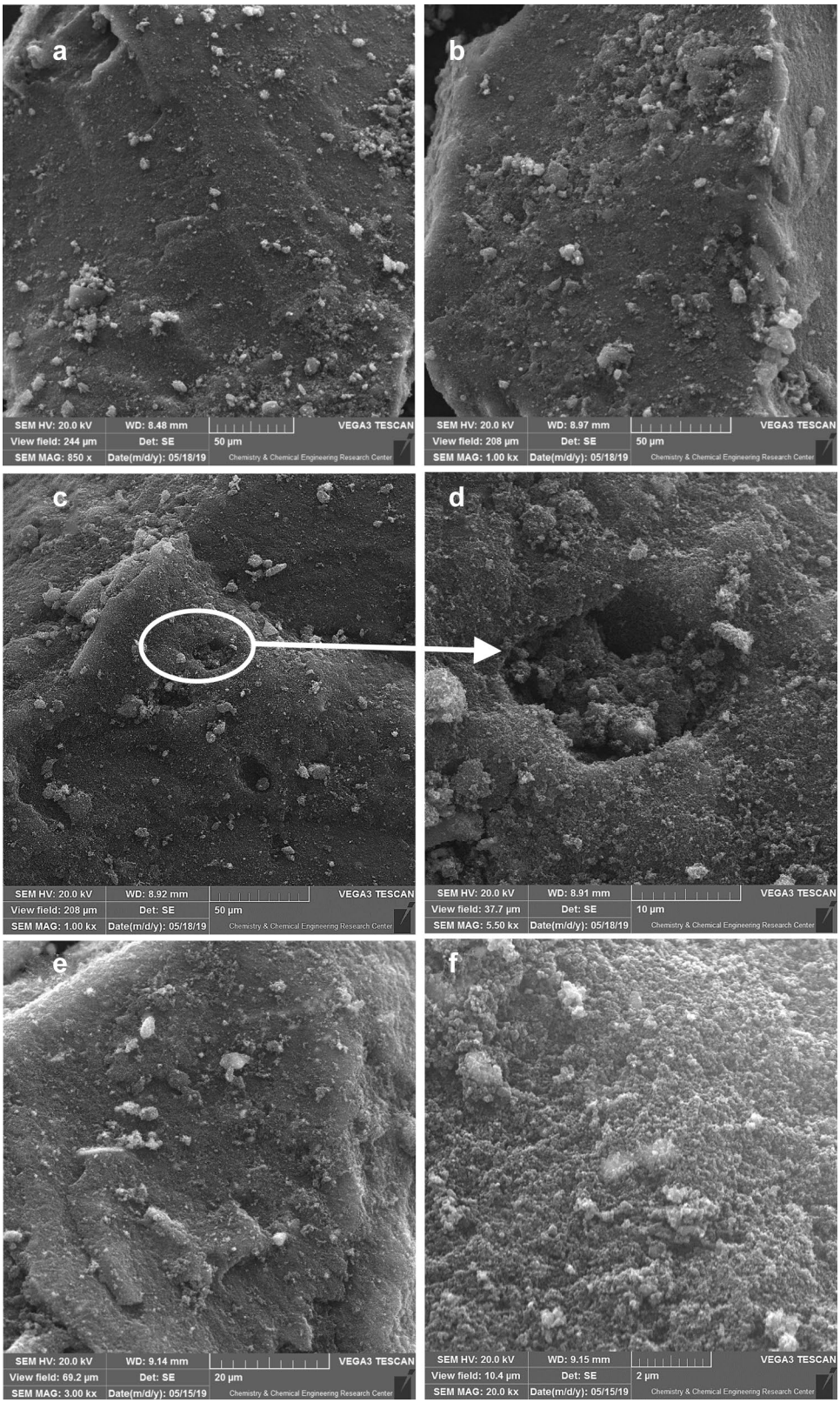

Fig. 3 Topographical SEM photos of **a** Pyrolysis char before activation and **b**–**f** activated carbon after steam activation in magnifications 1Kx, 1Kx, 5.5Kx, 3Kx, and 20Kx respectively

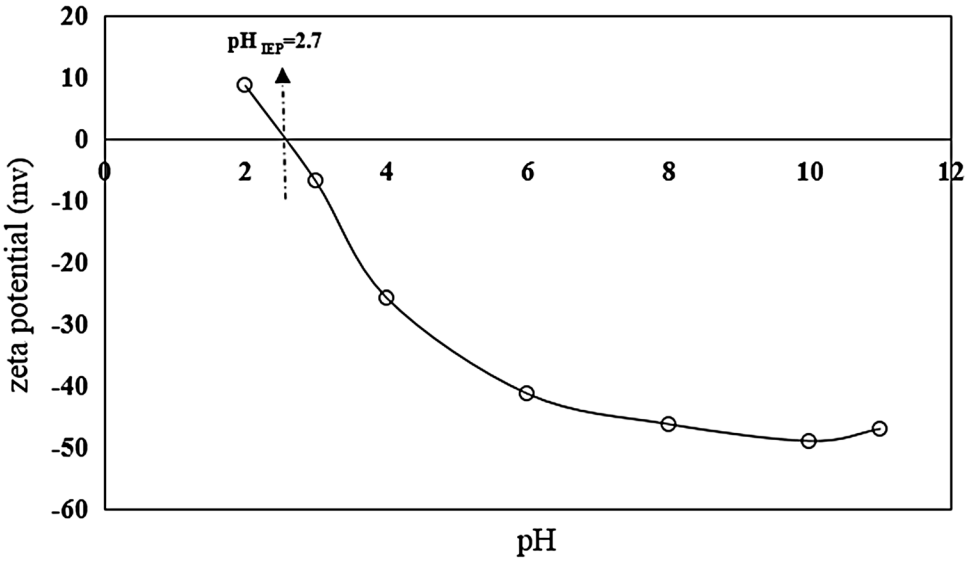

Fig. 4 Zeta potential curves versus pH of activated carbon

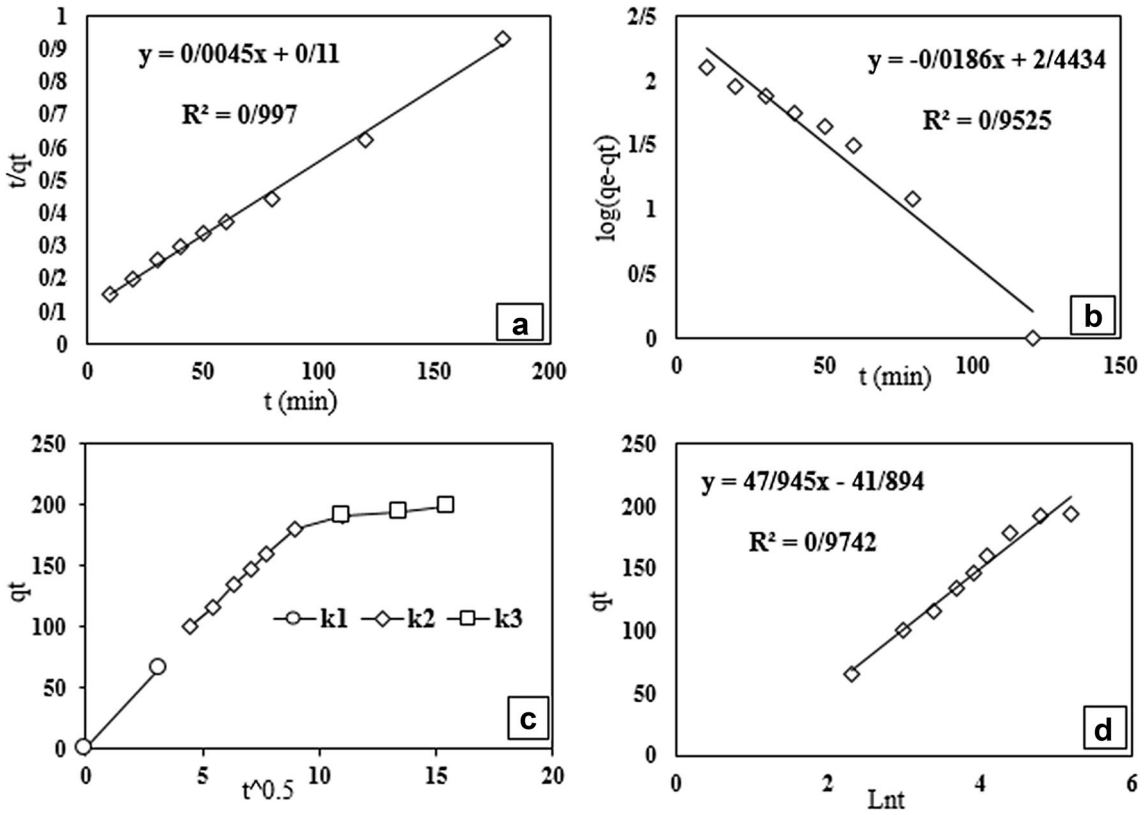

Fig. 5 The diagrams of various adsorption kinetics of MnO_4 by activated carbon. **a** Pseudo-second order kinetics **b** pseudo-first-order kinetics **c** diagram of particle diffusion kinetic **d** kinetic diagram of Elovich

values are very close and the error is minimum. Higher R^2_{Adj} values suggest the smaller disparity between theoretical and experimental q values.

Figure 5 shows the adsorption kinetic diagrams of different models. Models evaluated in Fig. 5a–d, are pseudo-second-order, pseudo-first-order, particle diffusion, and Elovich, respectively.

Table 1 Kinetic parameters of different kinetic models for MnO_4 adsorption on the absorbent

Pseudo-first-order			Pseudo-second order				Elovich			Particle diffusion					
K_1	q_e	R^2	R^2	h	K_2	q_e	α	β	R^2	Ki_3	R_3^2	Ki_2	R_2^2	Ki_1	R_1^2
0.01	11.51	0.95	0.00018	222.2	8.88	0.99	21.63	0.02	0.97	20.91	1	14.76	0.96	1.58	0.89

In this case, among the three studied models, the pseudo-second-order model presented the highest R^2_{Adj} values were 0.997 for all conditions described (see Table 1), which means that the qt predicted by the pseudo-second-order was the closest prediction to the values of qt measured experimentally.

The pseudo-second-order model includes the diffusion into the external film, particle diffusion, and interaction between metal ions and groups of adsorbent agents during the adsorption. Intraparticle diffusion is a transitional process that describes the motion of a mass fraction from solution to the solid phase. Also, the kinetic parameters of different kinetic models for MnO_4 adsorption on the adsorbent have shown in Table 1.

Figure 5c indicates that the adsorption process of MnO_4 includes more than one diffusion step. This figure shows that the values of k_i constants is as $k_{i,1}$ are $k_{i,2}$, $k_{i,3}$ (Sects. 2.4). This result shows that MnO_4 adsorption steps are in outer surface, inner surface, and equilibrium, respectively.

3.3 Equilibrium isotherms

Adsorption isotherms define how contaminants are bound to the adsorbent surface. They are essential to understand and optimize the utilization of a particular adsorbent. Also, the isotherms might help to comprehend better the mechanism of adsorption that will take place in the process [57]. There are several isotherm equations available for analyzing experimental adsorption equilibrium data, however, In this study, the Langmuir, Freundlich, Temkin, and D–R adsorption isotherms were evaluated for activated carbon (as adsorbent) efficiency in adsorbing MnO_4. The adsorption isotherms of MnO_4 onto activated carbons were performed using the following experimental conditions: temperature ranging from 25, 40, and 55 °C, pH 7.0, and adsorbent mass of 0.1 gr, and contact time between the adsorbent and adsorbate of 180 min. Figure 6 illustrates the adsorption isotherms and their fitness with various adsorption isotherm models.

Figure 6a shows the effect of temperature on adsorption capacity. By increasing temperature, the adsorption capacity increases. The maximum experimental values for MnO_4 of activated carbon were 120 mg/g. This enhancement in adsorption capacity could be due to the adsorbent surface activation. Also, this behavior can be explained because the temperature elevation can induce the increasing of thermal collisions and mobility of molecules in solution [61].

In Fig. 6b–e, the diagram of the linear form of the mentioned models has been drawn at 25, 40 and 55 °C. The constants of mentioned model are indicated in Table 2. As mentioned in Sect. 2.5, the isotherm equilibrium constant can be calculated according to the experimental data from the Eqs. 8, 9, 10, and 13 at any temperature.

For evaluation of experimental equilibrium data, the statistical analysis by the R^2_{Adj} is investigated, which presented in Table 2. In this regard, the Freundlich isotherm was the most suitable model for activated carbon. The Freundlich model exhibited the highest R^2_{Adj} values for activated carbon (see Table 2). This finding means that the q values obtained experimentally are very close to those q values calculated by the isotherm model [58, 59, 62]. The experimental equation of Freundlich isotherm is based on multilayers and non-homogeneous and heterogeneous adsorption of absorbed compound on the adsorbent [63].

The results obtained from the adsorption parameters showed in Table 2. It indicates the adsorption of MnO_4 on activated carbon by using physical method. These results are compatible with many others results reported in the literature which connects the textural properties of the adsorbent, as one of the main factors for obtaining a high adsorption performance [58, 64].

3.4 Thermodynamic of adsorption

Thermodynamic parameters of the adsorption of Mno_4 on the activated carbon were performed at the temperature ranging from 25 to 55 °C (298–328 K).

In Fig. 7, the logarithm of equilibrium constant is illustrated against the inverse of various temperature. As it shows, there is a linear relationship between the data. From the logarithmic fit of Eq. 15 to experimental data, the variations of enthalpy (ΔH) and entropy (ΔS) can be calculated. Subsequently, according to the Eq. 14 the Gibbs

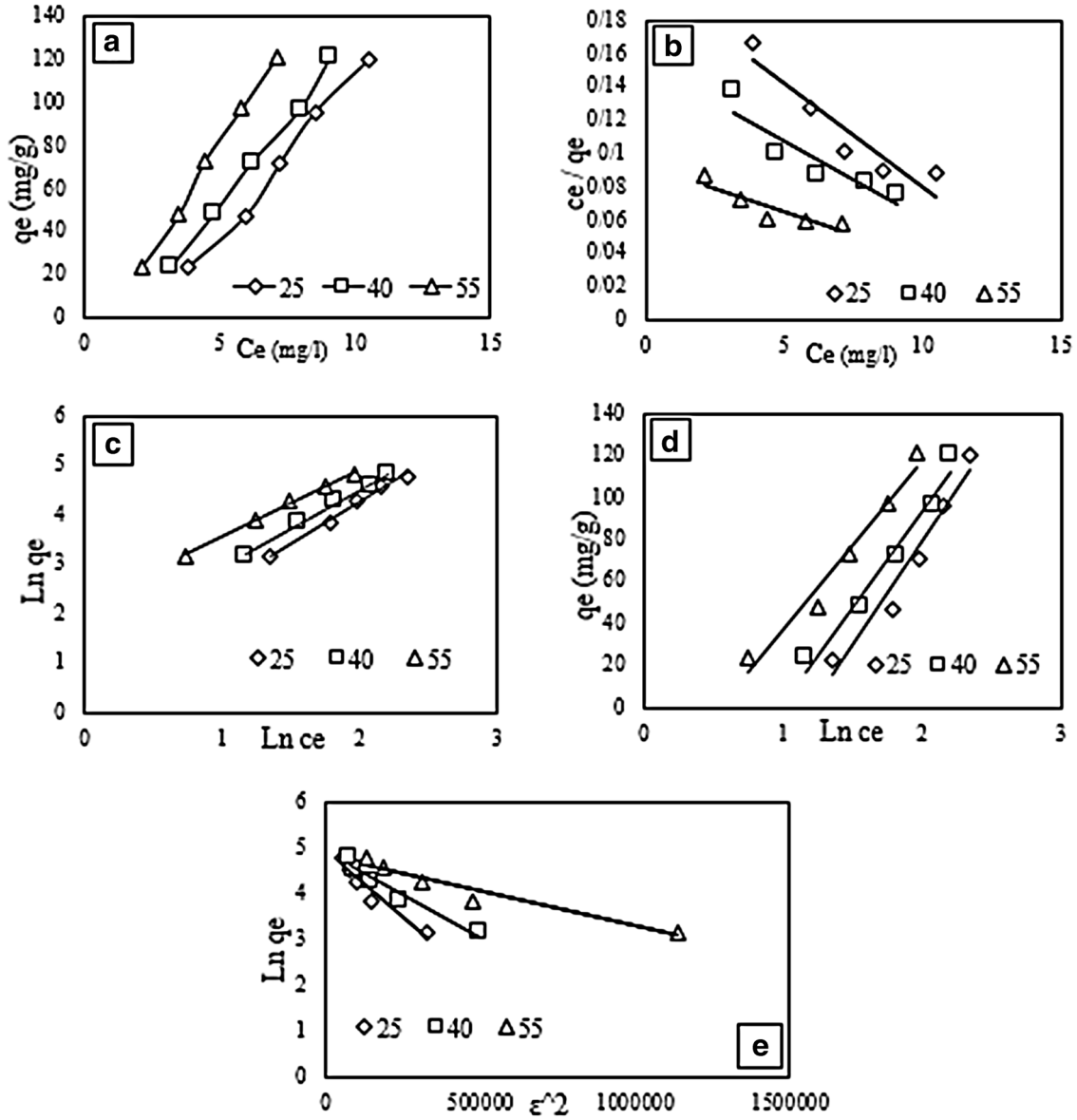

Fig. 6 the Adsorption isotherm diagrams, and it's fitting with various models at 25, 40 and 55 °C. **a** Adsorption isotherm diagram **b** Langmuir isotherm **c** Freundlich isotherm **d** Temkin Isotherm **e** D–R Isotherm

Table 2 Isotherm parameters of different isotherm models for MnO_4 adsorption on the absorbent

T (°C)	Freundlich			Langmuir			Temkin			D–R		
	n	k_f	R^2	q_m	K_1	R^2	b_T	A	R^2	B	q_m	R^2
25	0.74	9.09	0.992	12.72	0.38	0.87	2.12	4.62	0.95	6E−0.06	137.86	0.943
40	0.64	4.05	0.994	22.88	0.28	0.83	3.67	2.14	0.97	4E−0.06	135.42	0.96
55	0.59	2.36	0.99	33.44	0.32	0.79	5.72	5.62	0.96	2E−0.06	125.2	0.944

free energy variations can also be determined. The results of these calculations are shown in Table 3.

Table 3 shows that ΔG, ΔS, and ΔH have negative, positive, and positive values, respectively. The ΔG explains the thermodynamic process of adsorption with regards to its spontaneity; negative values for the ΔG indicate that the adsorption process of Mno_4 was energetically favorable and spontaneous at studied range of temperatures for activated carbon [62, 64–66].

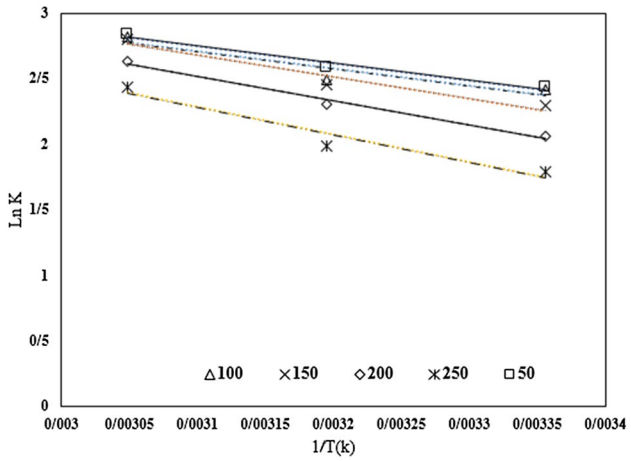

Fig. 7 The thermodynamic curve of LnK versus temperature

Table 3 Calculated values of thermodynamic equilibrium constant and Gibbs free energy

C (mg/l)	T (K)	ΔH (KJ/mol)	ΔS (KJ/mol)	ΔG (KJ/mol K)
50	298	10.837	0.0560	−4.438
	313			−5.172
	328			−6.447
100	298	10.889	0.0566	−5.104
	313			−5.981
	328			−6.647
150	298	13.811	0.0650	−5.673
	313			−6.373
	328			−7.645
200	298	15.375	0.0685	−5.986
	313			−6.474
	328			−7.692
250	298	17.382	0.0728	−6.032
	313			−6.720
	328			−7.741

Table 4 Mn adsorption capacity

Various articles	Mn adsorption capacity (mg/g)
Rajic et al. [22]	10
Jusoh et al. [23]	2.5451
Üçer et al. [24]	1.73
This article	120

Positive ΔS indicates the increasing accidental collides between the solid/liquid surface (adsorbent and soluble) during the adsorption process of MnO_4 [65–67].

Finally, the positive ΔH values show that the adsorption of Mno_4 on the activated carbon was an endothermic process. In addition, the ΔH values obtained were also found to be less than 17 kJ mol^{-1}; this further indicates the physical adsorption of Mno_4 on the activated carbon [68].

3.5 Comparisons of Mn adsorption capacity

Finally, In order to testify the effectiveness of the method, the results found in this work were compared with other methods reported. This comparison was shown in Table 4. As shown in the Table 4 According to the previous studies, the maximum adsorption of Mn was 10 mg/g while, the maximum adsorption obtained in this article was 120 mg/g.

4 Conclusion

In this study, the adsorption of Mn by activated carbon obtained from rusty tires was investigated. The adsorption and desorption porosimetry analysis, adsorption kinetics, isotherms, and thermodynamics evaluations were also carried out in this study. The adsorption and desorption porosimetry analysis showed that the maximum surface area for activated carbon achieved by the physical method was 550 m^2/gr. The results obtained from adsorption isotherms indicted their compatibility with Freundlich model. Based on the equilibrium calculations, the adsorption process has proceeded spontaneous and endothermic way. The results showed that the activated carbon (as adsorbent), produced by the physical procedure, has a good efficacy in adsorption of Mn.

Compliance with ethical standards

Conflict of interest The authors declare that they have no conflict of interest.

Ethical approval All authors have participated in (a) conception and design, or analysis and interpretation of the data; (b) drafting the article or revising it critically for important intellectual content; and (c) approval of the final version.

References

1. Dąbrowski A (2001) Adsorption-from theory to practice. J Adv Colloid Interface Sci 93(1):135–224
2. Sobhi N (1998) Removal of heavy metals from industrial wastewater by ash [dissertation]. Tarbiat Modarres University, Tehran
3. Dąbrowski A (2004) Selective removal of the heavy metal ions from waters and industrial wastewaters by ion-exchange method. J Chemosphere 56(2):91–106

4. Sarioglu M (2005) Removal of ammonium from municipal wastewater using natural Turkish (Dogantepe) zeolite. J Sep Purif Technol 41(1):1–11
5. Pirsaheb M, Dargahi A, Farrokhi M (2012) The efficiency of iron and manganese removal from groundwater using tower aeration. Zahedan J Res Med Sci 14:117
6. Esfandiar N, Nasernejad B, Ebadi T (2014) Removal of Mn(II) from groundwater by sugarcane bagasse and activated carbon (a comparative study): application of response surface methodology. J Ind Eng Chem 20:3726–3736
7. Xie M (2015) Synthesis and adsorption behavior of magnetic microspheres based on chitosan/organic rectorite for low-concentration heavy metal removal. J Alloys Compd 647:892–905
8. Meena AK (2005) Removal of heavy metal ions from aqueous solutions using carbon aerogel as an adsorbent. J Hazard Mater 122:161–170
9. bin Jusoh A (2005) Study on the removal of iron and manganese in groundwater by granular activated carbon. J Desalination 182:347–353
10. Tekerlekopoulou A, Vayenas D (2007) Iron and manganese removal from potable water using trickling filters. J Desalination 210:225–235
11. Wong K (2003) Removal of Cu and Pb by tartaric acid modified rice husk from aqueous solutions. J Chemosphere 50:23–28
12. Mohan S, Sreelakshmi G (2008) Fixed bed column study for heavy metal removal using phosphate treated rice husk. J Hazard Mater 153:75–82
13. Perret S (2000) Polarographic study of the removal of cadmium(II) and lead (II) from dilute aqueous solution by a synthetic flocculant. Comparison with copper(II) and nickel(II). J Water Res 34(14):3614–3620
14. Gonzalez-Munoz MJ (2006) Recovery of heavy metals from metal industry wastewaters by chemical precipitation and nanofiltration. J Desalination 200(1–3):742–744
15. Inglezakis VJ, Loizidou MD, Grgorooulou HP (2002) Equilibrium and kinetic ion exchange studies of Pb^{2+}, Cr^{3+}, Fe^{3+} and Cu^{2+} on natural clinoptilolite. J Water Res 36(11):2784–2792
16. Mier MV (2001) Heavy metal removal with Mexican clinoptilolite: multicomponent ionic exchange. J Water Res 35(2):373–378
17. Bouranenea S (2008) Influence of operating conditions on the rejection of cobalt and lead ions in aqueous solutions by a nano filtration polyamide membrane. J Membr Sci 325(1):150–157
18. Ritchie SMC, Bhattacharyya D (2002) Membrane-based hybrid processes for high water recovery and selective inorganic pollutant separation. J Hazard Mater 92(1):21–32
19. Shafaei A, Ashtiani FZ, Kaghazchi T (2007) Equilibrium studies of the sorption of Hg(II) ions onto chitosan. J Chem Eng 133(1):311–316
20. Qu JH (2008) Research progress of novel adsorption processes in water purification: a review. J Environ Sci 20(1):1–13
21. Chen JH (2010) Adsorption and desorption of Cu(II), Zn(II), Pb(II), and Cd(II) on the soils amended with nanoscale hydroxyapatite. J Environ Prog Sustain Energy 29(2):233–241
22. Rajic N (2009) Removal of aqueous manganese using the natural zeolite tuff from the Vranjska Banja deposit in Serbia. J Hazard Mater 172(2):1450–1457
23. Bin Jusoh A (2005) Study on the removal of iron and manganese in groundwater by granular activated carbon. J Desalination 182(1):347–353
24. Üçer A, Uyanik A, Aygün Ş (2006) Adsorption of Cu(II), Cd(II), Zn(II), Mn(II) and Fe(III) ions by tannic acid immobilized activated carbon. J Sep Purif Technol 47(3):113–118
25. Lin YR, Teng H (2002) Mesoporous carbons from waste tire char and their application in wastewater discoloration. J Micro Mesoporous Mater 54:167–174
26. San Miguel G, Fowler GD, Sollars CJ (2003) A study of the characteristics of activated carbons produced by steam and carbon dioxide activation of waste tyre rubber. J Carbon 41:1009–1016
27. Gupta VK, Rastogi A (2009) Biosorption of hexavalent chromium by raw and acid treated green alga *Oedogonium haiti* from aqueous solutions. J Hazard Mater 163:396–402
28. Mui ELK, Cheung WH, McKay G (2010) Tyre char preparation from waste tyre rubber for dye removal from effluents. J Hazard Mater 175:151–158
29. Gupta VK, Gupta B, Rastogi A, Agarwal S, Nayak A (2011) a comparative investigation on adsorption performances of mesoporous activated carbon prepared from waste rubber tire and activated carbon for a hazardous azo dye-Acid Blue 113. J Hazard Mater 186:891–901
30. Tanthapanichakoon W, Ariyadejwanich P, Japthong P, Nakagawa K, Mukai SR, Tamon H (2005) Adsorption–desorption characteristics of phenol and reactive dyes from aqueous solution on mesoporous activated carbon prepared from waste tires. J Water Res 39:347–355
31. Merchant AA, Petrich MA (1993) Pyrolysis of scrap tires and conversion of chars to activated carbon. J Environ Energy Eng 39:8
32. Allen JL, Gatz JL, Eklund PC (1999) Applications for activated carbons from used tires: butane working capacity. J Carbon 37:1485–1489
33. Zabaniotou AA, Stavropoulos G (2003) Pyrolysis of used automobile tires and rresidual char utilization. J Anal Appl Pyrolysis 70:711–722
34. Zabaniotou AA, Madau P, Oudenne PD, Jung CG, Delplancke MP, Fontana A (2004) Active carbon production from used tire in two-stage procedure: industrial pyrolysis and bench scale activation with H_2O–CO_2 mixture. J Anal Appl Pyrolysis 72:289–297
35. López G, Olazar M, Artetxe M, Amutio M, Elordi G, Bilbao J (2009) Steam activation of pyrolytic tyre char at different temperatures. J Anal Appl Pyrolysis 85:539–543
36. Ballhausen CJ (1962) Introduction to ligand field theory. Chemiker, Denmark
37. Atkins P, de Paula J (2010) Atkins Physical chemistry. Oxford University Press, New York
38. Almasifar D, Zarinabadi S (2009) Polarographic study of interactions between cadmium and lead ions and some chelating ligands in aqueous and no aqueous solvents. J Appl Res Chem 3:25–31
39. Melnick LM, Frieser H (1955) Extraction of metal thiocyanate complexes with tributyl phosphate. J Anal Chem 27:462–463
40. Baxendale JH, Gorge P (1950) Equilibria in solutions of ferrous ions and αα′- dipyridyl. J Trans Faraday Soc 46:55
41. Gan S, Jones B, Josrph H, Reibenspies R, Hancock D (2005) a fluorescent ligand rationally designed to be selective for zinc (II) over larger metal ions. The structures of the zinc (II) and cadmium (II) complexes of N, N-bis(2-methylquinoline)-2-(2-aminoethyl) pyridine. J Inorg Chim Acta 358:3958–3966
42. Labacz M, Stroka J, Galus Z (2005) The electrode reactions of several Pb(II)-macrocyclic complexes and their adsorption on mercury electrodes. J Electroanal Chem 582:109–117
43. Crouch AM, Khotseng LE, Polhuis M, Williams DR (2001) Comparative study of cyclic voltammetry with potentiometric analysis for determining formation constants for polyaminocarboxylate–metal ion complexes. J Anal Chem Acta 448:231–237
44. Wasay SA, Parker WJ, Van Geel PJ (2001) Contamination of a calcareous soil by battery industry wastes. I and II. Treatment. Can J Civ Eng 28(3):349–354
45. Lam KF, Yeung KL, McKay G (2007) Efficient approach for Cd^{2+} and Ni^{2+} removal and recovery using mesoporous adsorbent with tunable selectivity. J Environ Sci Technol 41(9):3329–3334

46. Algarra M, Jiménez MV, Rodríguez Castellón E, Jiménez-López A, Jiménez-Jiménez J (2005) Heavy metals removal from electroplating wastewater by aminopropyl-Si MCM-41. J Chemosphere 59(6):779–786
47. Hassan RM (1993) New coordination polymers. 111: oxidation of poly(viny1 alcohol) by permanganate ion in-alkaline solutions. kinetics and mechanism of formation of intermediate complex with a spectrophotometric detection of manganate (V1) transient species. J Polym Int 30:5–9
48. O'Shanness DJ, Winzor DJ (1996) Interpretation of deviations from pseudo-first-order kinetic behavior in the characterization of ligand binding by biosensor technology. J Anal Biochem 236(2):275–283
49. Ho YS, McKay G (1999) Pseudo-second order model for sorption processes. J Process Biochem 34(5):451–465
50. Zheng H (2008) Equilibrium, kinetic and thermodynamic studies on the sorption of 4-hydroxyphenol on Cr-bentonite. J Chem Eng 143(1):117–123
51. Javanbakht V (2016) A novel magnetic chitosan/clinoptilolite/magnetite nano composite for highly efficient removal of Pb(II) ions from aqueous solution. J Powder Technol 302:372–383
52. Foo K, Hameed B (2010) Insights into the modeling of adsorption isotherm systems. J Chem Eng 156(1):2–10
53. Anastopoulos I, Kyzas GZ (2016) Are the thermodynamic parameters correctly estimated in liquid-phase adsorption phenomena. J Mol Liq 218:174–185
54. Dotto GL, Santos JMN, Rodrigues IL, Rosa R, Pavan FA, Lima EC (2015) Adsorption of methylene blue by ultrasonic surface modified chitin. J Colloid Interface Sci 446:133–140
55. Gregg SJ, Sing KSW, Salzburg HW (1982) Adsorption surface area and porosity. Published by Academic Press, Inc. Ltd. London, 1967. 371 pages; $1820 (95 s)
56. Garten VA, Weiss DE, Willids JB (1957) A new interpretation of the acidic and basic structures in carbons. II. The chromene-carbonium ion couple in carbon. Aust J Chem 10:285
57. Lima EC, Adebayo MA, Machado FM (2015) Kinetic and equilibrium models of adsorption. Springer, Berlin, pp 33–69
58. Leite AB, Saucier C, Lima EC, dos Reis GS, Umpierres CS, Mello BL, Shirmardi M, Dias SLP, Sampaio CH (2018) Activated carbons from avocado seed: optimization and application for removal several emerging organic compounds. Environ Sci Pollut Res 25:7647–7661
59. Wamba AGN, Lima EC, Ndi SK, Thue PS, Kayem JG, Rodembusch GS, de Alencar WS (2017) Synthesis of grafted natural pozzolanwith 3-aminopropyltriethoxysilane: preparation, characterization, and application for removal of Brilliant Green 1 and Reactive Black 5 from aqueous solutions. Environ Sci Pollut Res 24:21807–21820
60. Saucier C, Karthickeyan P, Ranjithkumar V, Lima EC, dos Reis GS, de Brum IAS (2017) Efficient removal of amoxicillin and paracetamol from aqueous solutions using magnetic activated carbon. Environ Sci Pollut Res 24:5918–5932
61. Sellaoui L, Dotto GL, Gonçalves JO, Pinto LAA, Knani S, Lamine AB (2016) Equilibrium modeling of single and binary adsorption of Food Yellow 4 and Food Blue 2 on modified chitosan using a statistical physics theory: new microscopic interpretations. J Mol Liq 222:151–158
62. Prola LDT, Machado FM, Bergmann CP, de Souza FE, Gally CR, Lima EC, Adebayo MA, Dias SLP, Calvete T (2013) Adsorption of Direct Blue 53 dye from aqueous solutions by multi-walled carbon nanotubes and activated carbon. J Environ Manag 130:166–175
63. Freundlich H (1907) Über die adsorption in lösungen. Z Phys Chem 57:385–470
64. Umpierres CS, Thue PS, dos Reis GS, de Brum IAS, Lima EC, de Alencar WA, Dias SLP, Dotto GL (2018) Microwave activated carbons from Tucumã (*Astrocaryum aculeatum*) waste for efficient removal of 2-nitrophenol from aqueous solutions. J Environ Technol 39:1173–1187
65. Thue PS, Adebayo MA, Lima EC, Sieliechi JM, Machado FM, Dotto GL, Vaghetti JCP, Dias SLP (2016) Preparation, characterization and application of microwave-assisted activated carbons from wood chips for removal of phenol from aqueous solution. J Mol Liq 223:1067–1080
66. Saucier C, Adebayo MA, Lima EC, Cataluna R, Thue PS, Prola LDT, Puchana-Rosero MJ, Machado FM, Pavan FA, Dotto GL (2015) Microwave-assisted activated carbon from cocoa shell as adsorbent for removal of sodium diclofenac and nimesulide from aqueous effluents. J Hazard Mater 289:18–27
67. Ocampo-Perez R, Aguilar-Madera CG, Díaz-Blancas V (2017) 3D modeling of overall adsorption rate of acetaminophen on activated carbon pellets. Chem Eng J 321:510–520
68. Sun CL, Wang CS (2010) Estimation on the intramolecular hydrogen bonding energies in proteins and peptides by the analytic potential energy function. J Mol Struct 956:38–43